Electromagnetically Driven Torsional Resonators for Viscosity and Mass Density Sensing Applications Electromagnetically Driven Torsional Resonators for Viscosity and Mass Density Sensing Applications

M Heinisch, T Voglhuber-Brunnmaier, Erwin Reichel, I Dufour, B Jakoby

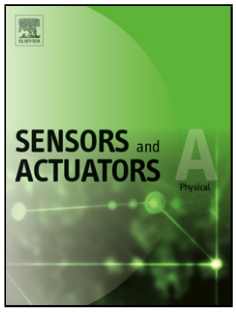

Title: Electromagnetically Driven Torsional Resonators for Viscosity and Mass Density Sensing Applications

Author: M. Heinisch T. Voglhuber-Brunnmaier E.K. Reichel I. Dufour B. Jakoby

PII: S0924-4247(15)00156-9
DOI: http://dx.doi.org/doi:10.1016/j.sna.2015.03.033
Reference: SNA 9131

To appear in: *Sensors and Actuators A*

Received date: 8-10-2014
Revised date: 6-3-2015
Accepted date: 26-3-2015

Please cite this article as: M. Heinisch, T. Voglhuber-Brunnmaier, E.K. Reichel, I. Dufour, B. Jakoby, Electromagnetically Driven Torsional Resonators for Viscosity and Mass Density Sensing Applications, *Sensors & Actuators: A. Physical* (2015), http://dx.doi.org/10.1016/j.sna.2015.03.033

Electromagnetically Driven Torsional Resonators for Viscosity and Mass Density Sensing Applications

M. Heinisch[a], T. Voglhuber-Brunnmaier[a,b], E.K. Reichel[a], I. Dufour[c], B. Jakoby[a]

[a] *Institute for Microelectronics and Microsensors, Johannes Kepler University, Linz, Austria*
[b] *Center for Integrated Sensors Systems, Danube University, Krems, Austria*
[c] *Université de Bordeaux, Laboratoire de l'Intégration du Matériau au Système, Pessac, France*

Abstract

In this contribution a conceptual study for torsional oscillators, which are electromagnetically driven and read out, is presented. The aim is to experimentally investigate the basic feasibility of a torsional resonator with application to viscosity and mass density sensing in liquids. Such a device is particularly interesting as cylindrical, torsional resonators for fluid sensing applications are hardly reported but unlike many other devices, yield pure shear wave excitation in the liquid. The design of first conceptual demonstrators for measurements in air as well as in liquids and their benefits and disadvantages are discussed in detail. A closed form as well as a reduced order model and measurement results obtained with first demonstrators are presented.

Keywords: Torsional, resonator, cylinder, shear wave, viscosity, mass density

1. Introduction

Recently, we investigated various resonant sensors for liquid viscosity and mass density, see e.g., [1], which were particularly designed to be operated in the low kilohertz range. Amongst these devices, in-plane oscillating platelets, emitting mainly shear waves into the sample liquids, were investigated e.g., in [2, 3] where millimeter sized metal platelets were used. In [4, 5] similar miniaturized devices have been implemented in silicon technology. Generally used shear oscillating resonators, such as shear oscillating quartz crystals [6] and the aforementioned in-plane oscillating platelets, have in common that, besides the desired shear waves, compressional waves are also radiated into the liquid. These pressure waves result e.g., from non-uniform shear displacement [7, 8], the resonators' finite thicknesses, and spurious out-of-plane modes e.g. from the plate itself or of supporting beams. Potential candidates for resonators which only emit shear waves into the test fluid are cylindrical torsional oscillators. First, such pure shear wave emitting devices are of special interest from a rheological point of view, when it comes to the analysis of complex liquids such as viscoelastic liquids. For pure shear wave deformation, the liquid can be described by a complex-valued shear modulus or a complex valued viscosity, which, in general, are frequency dependent quantities [9]. With oscillatory measurements, the values obtained at a number of discrete frequencies can be used to obtain a rheological spectrum. A second merit for cylindrical, torsional resonators is that, due to their geometry, they resemble concentric cylinder rheometers. Thus, they yield comparable measurements but extend the measurable frequency range of conventional rheometers which is usually limited at approximately 100 Hz. Third, cylindrical, torsional oscillators allow experimental comparison of measurement results obtained with the above mentioned in-plane oscillating resonators, which excite spurious compressional waves. Thus, by means of such a comparison the impact of these compressional waves could be experimentally estimated.

In-plane oscillating devices, oscillating rotational disks [10] and other resonators for viscosity and mass density sensors such as cantilevers [11, 12], quartz tuning forks [13] and vibrating bridges [14, 15] are based on a similar operational principle. Usually, the devices' frequency responses, containing a characteristic resonant mode, are recorded upon immersion in a sample liquid. The change of evaluated resonance frequencies and quality factors are then related to the liquid's mass density and viscosity.

In this work a feasibility study for electromagnetically driven and read out torsional oscillators for operation in liquids is presented. Two concepts for actuation and readout discussed in Sec. 2 were manufactured and the experimental analysis in air allowed investigating the benefits and disadvantages of both approaches. The analysis of measurements obtained with three different torsional spring diameters and various spring lengths allowed designing a demonstrator for measurements in liquids, which is explained in detail in Sec. 3. A closed form model for the resonator, relating the input to the output voltage, is derived in Sec. 4. In Sec. 5 evaluated results of measurements obtained with the cylindrical torsional resonator in ten different liquids are shown. Furthermore, the sensor's sensitivity and cross sensitivity to temperature are evaluated and compared to other sensor concepts.

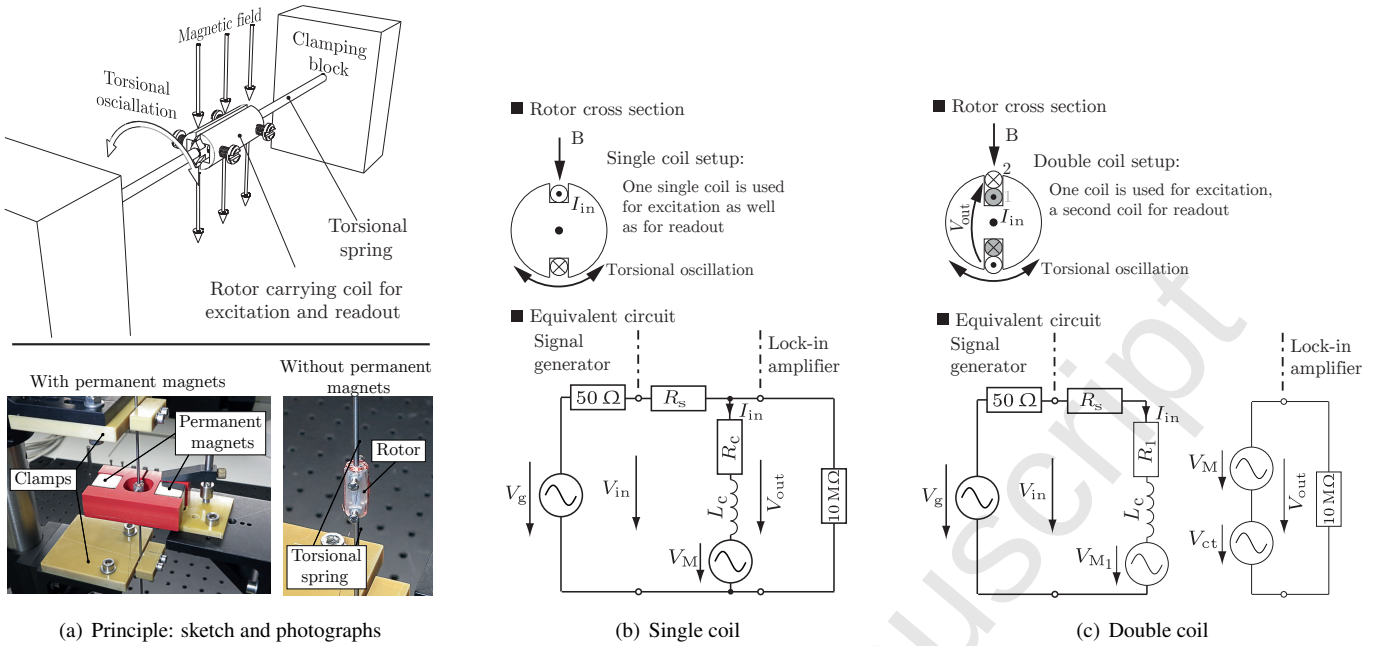

(a) Principle: sketch and photographs (b) Single coil (c) Double coil

Figure 1: a) Principle and photographs of first demonstrators allowing to record frequency responses in air, b) cross section and electrical equivalent circuit of the demonstrator with a rotor carrying a single coil for excitation and readout by means of Lorentz-forces. I_{in}: input (excitation) current, B: external magnetic field, V_g: voltage of the signal generator, 50 Ω: output resistance of the signal generator, R_s: series resistance, R_c, L_c: coil's resistance and inductance, V_M: motion induced voltage, 10 MΩ: input resistance c) cross section and electrical equivalent circuit of the rotor carrying two coils. One coil is used for excitation, the other for read out., V_{ct}: induced voltage due to inductive crosstalk.

2. Torsional resonator

2.1. Concept

The basic idea of the torsional resonator is to excite a cylinder to torsional vibrations by means of Lorentz forces acting on sinusoidal currents in a constant external magnetic field. For recording the device's frequency response, the excitation current's frequency is swept over a frequency range containing the resonant fundamental mode and simultaneously measuring the motion induced voltage on an electrical conductor, following the torsional oscillation. To implement this idea, a rotor (bobbin) is mounted on torsional springs, where two different principles were realized and compared. In the first approach, the bobbin carries one single coil which is used for both, excitation and read out, where in the second approach, two separate coils are used for these tasks.

2.2. Conceptual investigation in air

To investigate the functional principle of the electromagnetic torsional oscillator and to estimate the achievable range of resonance frequencies and signal strengths, a single coil type bobbin has been mounted and investigated on three torsional springs at various spring lengths. For this, a setup as depicted in Figs. 1(a) and 1(b) has been used. There, one hundred turns of a 80 µm thick copper wire were wound on a 3D printed bobbin with 8 mm in diameter and 22 mm in length, which was attached to tungsten rods with diameters of 0.58 mm, 1.6 mm and 2 mm serving as torsional springs. For each torsional spring, the same rotor was used so that only the effect of different torsional spring lengths and diameters could be examined. For attaching, the rotor was affixed with screws to the torsional springs, which were rigidly clamped at their ends with fibreglass blocks through which the torsional spring lengths could be adjusted. The bobbin was placed in a magnetic field (denoted with B) provided by neodymium permanent magnets and set to torsional oscillations by means of Lorentz forces on sinusoidal currents (I_{in}) in the coil which was connected to a signal generator (V_g and 50 Ω output resistance) and a series resistance $R_s = 100\,\Omega$ which was used to limit the excitation current, to prevent from non-linear deflections. By sweeping the excitation current's frequency, the oscillator's frequency response can be recorded. In this case, for the sake of straight forward manufacturing, the coil's ends of the 80 µm thick copper wire were kept long enough for direct connection with the excitation and readout electronics. However, for a stable resonator, this wiring approach is not adequate. In the demonstrator used for measurements in liquids which will be presented in Sec. 3 this drawback has been overcome by connecting the coil's ends to the torsional springs for electrical connection of the resonator.

Figure 2 shows the results of recorded frequency responses and evaluated resonance frequencies in air for tungsten rods with diameters of 0.58 mm and 1.6 mm for various spring lengths in comparison with theoretical results also presented in [16]. These results proved the basic feasibility of the concept and allowed designing a torsional resonator in the desired frequency range.

2.3. Single versus double coil setup

The benefits and disadvantages of using single or double coil setups were experimentally investigated. The cross sec-

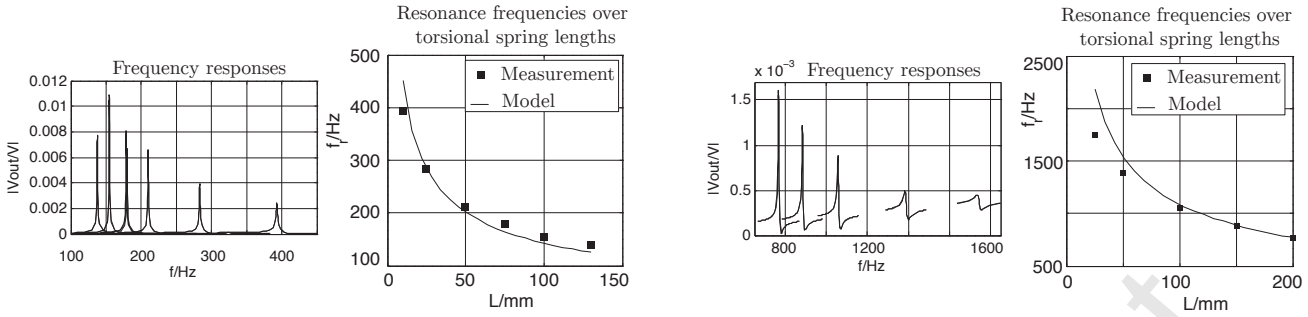

(a) Spring diameter 0.58 mm (b) Spring diameter 1.6 mm

Figure 2: Examples for recorded frequency responses in air using a single coil for excitation and read-out. These experiments were performed to estimate achievable signal strengths and resonance frequencies for different spring diameters and spring lengths.

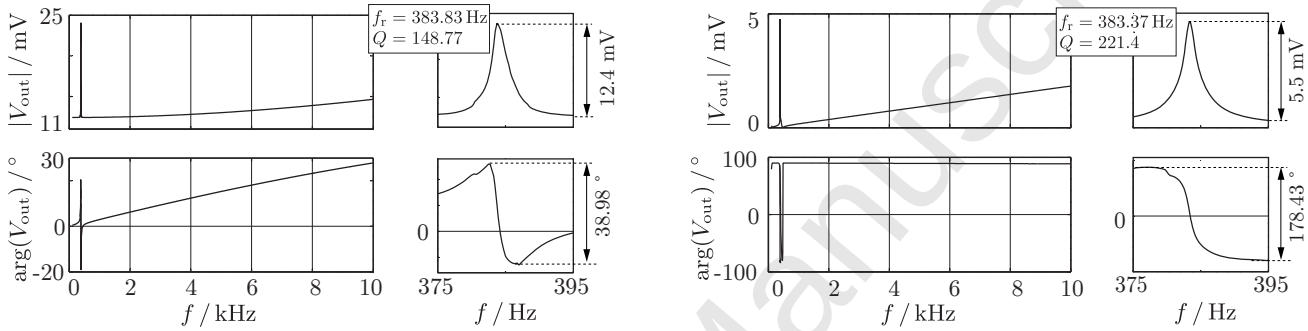

(a) Single coil (b) Double coil

Figure 3: Frequency responses measured with the single coil (a) and the double coil (b) setup. The recorded spectra between 100 Hz and 10 kHz as well as detailed plots of the resonance are shown for both setups.

tions of the rotors as well as the electrical equivalent circuits for both cases are depicted in Figs. 1(b) and 1(c). For the first case, a single coil with 100 turns, a length of 20 mm and a width of 8 mm is used for both, excitation and read out and for the second case, two coils with 50 turns each are used separately for these purposes. The voltage of the signal generator V_g was 0.1 V and the series resistance R_s was 100 Ω.

For the single coil setup, the rotor is excited to torsional vibrations by means of Lorentz forces on sinusoidal currents I_{in}. The oscillation of the coil in the presence of the external magnetic field causes a motion induced voltage V_M on the excitation coil itself. This motion induced voltage is proportional to the the velocity of the oscillation and thus an appropriate quantity for measuring the oscillation. However, the measurable output voltage V_{out} consists of an additional voltage resulting from the coil's impedance related voltage drop. The coil's impedance is modeled as a serial connection of a resistance R_c and an inductance L_c. For the manufactured rotor $R_c = 21.3\,\Omega$ and $L_c = 215\,\mu H$ were obtained by fitting the parameters in the recorded frequency response from 100 Hz to 100 kHz. The output voltage was measured with a lock-in amplifier (with an input resistance of 10 MΩ) and reads

$$\underline{V}_{out}(\omega) = \underline{V}_M(\omega) + (R_c + j\,\omega\,L_c)\underline{I}_{in} \quad (1)$$

in complex notation where $j = \sqrt{-1}$, ω is the angular frequency and the time dependence $e^{j\omega t}$ is suppressed.

To reduce this impedance-related offset voltage, a second coil is used in the double coil setup for readout. This second coil follows the motion of the oscillating cylinder and thus, as in the single coil setup, a voltage is induced. However, in this case due to electrical crosstalk resulting from the current I_{in} in the excitation coil, an additional voltage V_{ct} is induced in the measuring coil. Assuming that the output current I_{out} is negligible, the output voltage reads

$$\underline{V}_{out}(\omega) = \underline{V}_M(\omega) + j\,\omega\,M\,\underline{I}_{in} \quad (2)$$

where M is the mutual inductance describing the inductive coupling from the excitation to the readout coil. For the rotor used in this experiment $M = 480\,\mu H$ was obtained.

Both types of rotors have been manufactured and mounted on a tungsten rod with 0.58 mm diameter and 5 cm length for each torsional spring. The recorded frequency responses covering a frequency range of 100 Hz to 10 kHz as well as detailed plots of the fundamental resonance are shown in Fig. 3 for both cases. The resonance peak is more than twice as high in case of the single coil setup compared with the double coil setup. (12.4 mV in contrast to 5.5 mV for the double coil setup.) This results from the fact that for the single coil setup, the number of coil turns is twice as high which yields a higher effective driving force in the rotor and a proportional to the coil turns higher induced voltage. Thus, assuming the same mechanical conditions for both setups, the voltage peak of the single coil setup

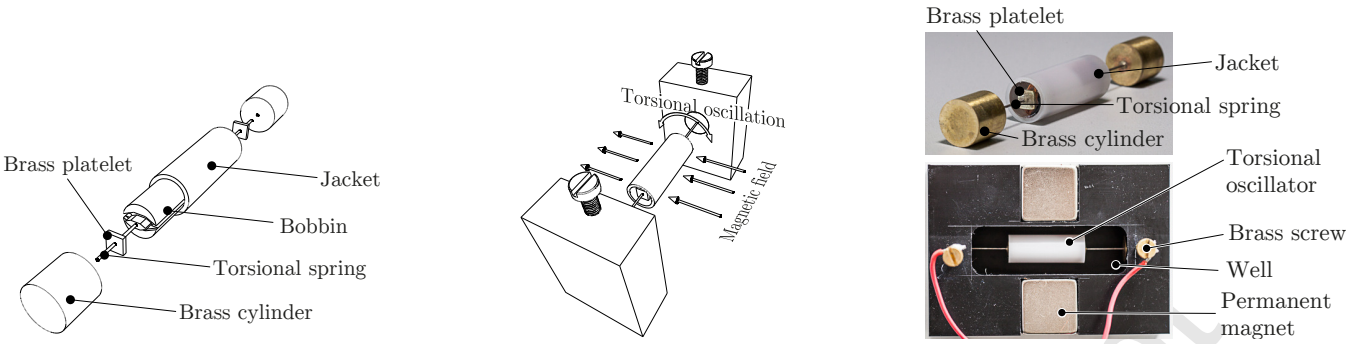

(a) Exploded illustration (b) Assembled, clamped illustration (c) Photographs

Figure 4: a) Exploded view of the torsional resonator used for measurements in liquids. The coil is electrically connected via the torsional springs and the brazed brass cylinders, which are clamped with brass screws to which connecting wires are soldered. b) shows an illustration of the assembled, clamped setup, the direction of the external magnetic field as well as the torsional oscillation. c) The upper photograph shows the manufactured torsional oscillator. The lower photograph shows the complete setup including both permanent magnets and the torsional oscillator placed in the experimental well which was filled with the sample liquids.

should be four times as high as the double coil setup. However, in the performed experiments, this is not the case, as the quality factor of the single coil setup (Q = 148.77) is significantly smaller than in case of the double coil setup (Q = 221.4). Due to the large offset voltage for the single coil ($\approx$ 12 mV) the change of phase at resonance is significantly smaller as for the double coil (38.98° in comparison to 178.43°). The reason of the phase shift of 178.43° instead of supposedly 180° is that the output voltage is subjected to a slight crosstalk voltage at these frequencies. This crosstalk voltage increases proportionally to the excitation frequency as it can be observed in Fig. 3(b) which is also considered in Eq. 2.

3. Demonstrator for measurements in liquids

The use of a second coil did not show a major advantage in the obtained signals compared to the setup where only one coil is used for excitation and readout. However, using only one coil has a significant advantage for electrical connection. In this case, the electrical conductive torsional springs can be used for this task. For the double coil setup which requires the connection of four wires, the usage of tubes would be necessary (serving as torsional springs) through which the coils' wires have to be threaded which might be a rather tedious manufacturing process. Fig. 4 shows drawings and photographs of the torsional resonator with which first measurements in ten different liquids were obtained.

As for the single coil type rotor, which was investigated in air, one hundred turns of a copper wire with a diameter of 80 µm were wound on a 3D printed bobbin. Two tungsten rods with a diameter of 0.58 mm serve as torsional springs with a spring length of 14 mm each. Each rod is brazed to a brass cylinder with 10 mm diameter and 10 mm height. Both tungsten rods carry a brazed brass platelet and are put into the bobbin on both sides ensuring no contact of both torsional springs. Each end of the coil is glued with electrical conductive glue to one of these brass platelets which are furthermore used for a form-fitted connection with epoxy resin poured into both sides of the bobbin which in turn is put into a POM-C (polyacetal) plastics jacket with an outer diameter of 10 mm and 25 mm length. As mentioned before, it is essential that the tungsten rods do not get in contact in order not to shortcut the coil. The torsional resonator is put into a milled POM-C plastics frame with a well for containing the sample liquids. The brass cylinders are clamped with brass screws, which in turn are used for further electrical connection for power supply and read-out. Two neodymium magnets are used for providing a magnetic field necessary for excitation and read-out based on Lorentz-forces.

4. Modeling

4.1. Mechanical model

4.1.1. Structural mechanics

Considering the rotor's moment of inertia J_0, the torque resulting from the tungsten rods' torsional stiffnesses M_T, the excitation torque M_ex, a torque M_c, representing the intrinsic dissipative losses of the resonator and a torque M_F accounting for the torque due to the liquid loading, the principle of momentum equilibrium yields, cf. Fig. 5

$$J_0 \frac{\mathrm{d}^2\varphi(t)}{\mathrm{d}t^2} + 2\,M_\mathrm{T} + M_\mathrm{c} + M_\mathrm{F} = M_\mathrm{ex} \tag{3}$$

where φ is the twisting angle of the rotor.

For a cylindrical rod with shear modulus G, radius r_s, length l_s and twisting angle φ the torsional torque reads [17]

$$M_\mathrm{T} = k_\mathrm{T}^*\,\varphi. \tag{4}$$

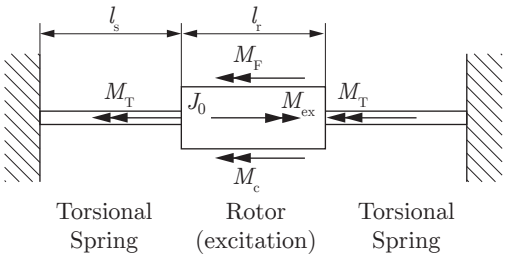

Figure 5: Torques considered in the principle of moment equilibrium. A double arrow illustrates an acting torque.

where

$$k_{\mathrm{T}}^{*} = G\,\frac{\pi}{2}\,\frac{r_{\mathrm{s}}^{4}}{l_{\mathrm{s}}}. \tag{5}$$

is the torsional spring constant of one torsional spring and $k_{\mathrm{T}} = 2\,k_{\mathrm{T}}^{*}$ is the spring constant of both torsional springs in our case.

Dissipative losses are considered by a loss coefficient c_0 and the associated loss torque is

$$M_{\mathrm{c}} = c_0\,\frac{\mathrm{d}\varphi}{\mathrm{d}t}. \tag{6}$$

4.1.2. Fluid dynamics

As we are facing a rotational problem, the solution of the fluid forces acting on the oscillating cylinder contains Hankel functions which make the obtained equations difficult to interpret. For this reason, the fluid forces acting on the cylinder are approximated by one dimensional shear waves of an in-plane oscillating plate which yields a negligible error if the cylinder's radius r_{c} is significantly larger than the penetration depth [18], also termed decay length [6]

$$\delta = \sqrt{\frac{2\eta}{\rho\,\omega}} \tag{7}$$

where η and ρ are the liquid's viscosity and mass density, respectively and ω is the angular frequency of the oscillation.

A comparison of the relative deviations ε of the solutions for the cylindrical and the planar case over the ratio r_{c}/δ are depicted in Fig. 6. The complete derivation for the fluid forces is only given for the planar case in this contribution. For aqueous liquids at 1 kHz the penetration depth is 18 µm approximately. Considering the cylinder's radius of the manufactured demonstrator $r_{\mathrm{c}} = 5$ mm it follows $r_{\mathrm{c}}/\delta = 280$ and thus $\varepsilon = 3.8 \cdot 10^{-3}$ which substantiates the applicability and the validity of the approximated solution.

Under the assumptions of an infinitely extended plate oscillating only in x-direction (thus imposing only shear stress in x-direction), that gravitational forces are negligible, and that the liquid is incompressible, the equation of motion and the shear stress T_{xz} in liquids can be expressed as a one dimensional problem and reads [6, 19]:

$$\rho\,\frac{\partial^2 u_x}{\partial t^2} = \frac{\partial T_{xz}}{\partial z} \qquad \text{with} \qquad T_{xz} = \eta\frac{\partial^2 u_x}{\partial z\,\partial t}. \tag{8}$$

Here, ρ is the mass density of the liquid, u_x is the displacement of the liquid in x-direction, t is the time variable.

Substituting T_{xz} in the equation of motion, transforming the problem to the frequency domain assuming a time dependence $e^{j\omega t}$ and solving the linear differential equation of second order yields the solution for the x-displacement propagating in z-direction

$$\underline{u}_x(z,t) = u_0\,e^{-\frac{z}{\delta}}\,e^{-j\left(\frac{z}{\delta}-\omega t\right)} \tag{9}$$

where u_0 is the amplitude of the oscillation. With this solution for $\underline{u}_{\mathrm{x}}$, the shear stress at the liquid-solid interface (i.e., $z = 0$) in the frequency domain reads

$$\underline{T}_{xz}(z=0) = \underline{u}_x\,(1-j)\,\sqrt{\frac{\eta\rho\,\omega^3}{2}}. \tag{10}$$

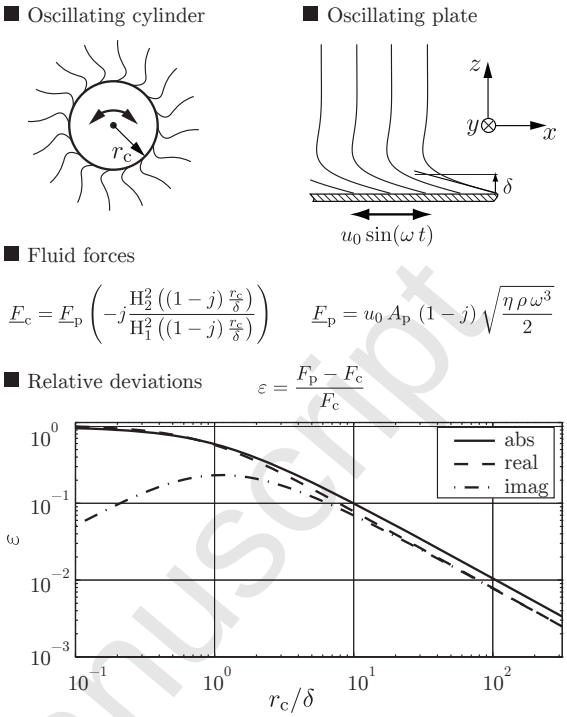

Figure 6: Comparison of the solutions for the fluid forces F_{c} and F_{p} acting on an oscillating cylinder and an in-plane oscillating plate, respectively. For both cases, the same surface interacting with the liquid is considered. In case of the solution for the cylinder, Hankel functions are obtained which make an intuitive interpretation of the obtained equations difficult. For high ratios of the cylinder's radius r_{c} and the penetration depth δ, the difference between both solutions is negligibly small.

Expressing the planar deflection in rotational form, i.e. $u_{\mathrm{x}} \rightarrow \varphi\,r_{\mathrm{c}}$ and assuming $M_{\mathrm{F}} = -r_{\mathrm{c}}\,T\,A_{\mathrm{c}}$, where A_{c} is the cylinder's surface, the torque acting on the oscillating cylinder can be expressed as

$$\underline{M}_{\mathrm{F}} = \left[-\omega^2\sqrt{\frac{\eta\rho}{2\,\omega}}\,r_{\mathrm{c}}^2\,A_{\mathrm{c}} + \mathrm{j}\omega\sqrt{\frac{\eta\rho\,\omega}{2}}\,r_{\mathrm{c}}^2\,A_{\mathrm{c}}\right]\underline{\varphi}(\omega). \tag{11}$$

Eqs. 4 and 6 are substituted in Eq. 3. and after transformation of the obtained expression to the frequency domain, Eq. 11 can be considered in the equation of the moment equilibrium

$$\left[-\omega^2\,J + k_{\mathrm{T}} + \mathrm{j}\omega\,c\right]\underline{\varphi}(\omega) = \underline{M}_{\mathrm{ex}} \tag{12}$$

where J and c have been introduced and read

$$J = J_0 + \sqrt{\frac{\eta\rho}{2\,\omega}}\,r_{\mathrm{c}}^2\,A_{\mathrm{c}} \quad \text{and} \quad c = c_0 + \sqrt{\frac{\eta\rho\,\omega}{2}}\,r_{\mathrm{c}}^2\,A_{\mathrm{c}}. \tag{13}$$

As the torsional resonator is operated close to its (fundamental) angular resonance frequency ω_0, these expressions can be approximated by

$$J \approx J_0 + \sqrt{\frac{\eta\rho}{2\,\omega_0}}\,r_{\mathrm{c}}^2\,A_{\mathrm{c}} \quad \text{and} \quad c \approx c_0 + \sqrt{\frac{\eta\rho\,\omega_0}{2}}\,r_{\mathrm{c}}^2\,A_{\mathrm{c}}. \tag{14}$$

Substituting these relations into Eq. 12 yields a closed form model of the oscillating cylinder in liquids and is beneficial for design purposes. However, as the model consists of a relatively

large amount of variables, which are usually not exactly known, constants and variables are combined in single factors where possible to reduce the amount of variables which have to be determined in a parameter fit.

4.2. Reduced order models

4.2.1. One dimensional shear waves

Combining factors and variables in Eq. 14 in single factors and neglecting the ω_0 dependence allows writing J and c in reduced form as follows

$$J \approx J_0 + J^*_{\eta\rho}\,\sqrt{\eta\rho} \quad \text{and} \quad c \approx c_0 + c^*_{\eta\rho}\,\sqrt{\eta\rho}. \tag{15}$$

With this, the angular speed $\underline{\Omega}(\omega) = j\omega\underline{\varphi}(\omega)$ can be expressed as

$$\underline{\Omega}(\omega) = \frac{\underline{M}_{ex}/c}{1 + j\,Q\left(\frac{\omega}{\omega_0} - \frac{\omega_0}{\omega}\right)} \tag{16}$$

with angular resonance frequency

$$\omega_0 = \sqrt{\frac{k_\mathrm{T}}{J}} = \frac{1}{\sqrt{J_{0\mathrm{k}} + J^*_{\eta\rho\mathrm{k}}\,\sqrt{\eta\rho}}} \tag{17}$$

and quality factor

$$Q = \frac{\sqrt{J\,k_\mathrm{T}}}{c} = \frac{1}{\omega_0}\frac{k_\mathrm{T}}{c} = \frac{\sqrt{J_{0\mathrm{k}} + J^*_{\eta\rho\mathrm{k}}\,\sqrt{\eta\rho}}}{c_{0\mathrm{k}} + c^*_{\eta\rho\mathrm{k}}\,\sqrt{\eta\rho}}. \tag{18}$$

where the subscript k denotes that the factors in Eq. 15 have been divided by k_T to obtain these solutions for ω_0 and Q.

For resonators, which are readout via a motion induced voltage (which is proportional to the oscillator's velocity, see Sec. 4.3.2) the maximum peak frequency and the frequency of free, undamped oscillations (usually termed ω_0) are identical. For this reason, we may call ω_0 resonance frequency. For read-out principles evaluating the resonator's deflection using e.g. optical methods [20], the frequency of free, undamped oscillations and the maximum peak frequency of deflection amplitude are not identical.

4.2.2. Generalized model

In [21] a similar reduced order model was presented which considers not only one dimensional shear waves but convexly shaped, oscillating objects in general and reads

$$\omega_0 = \frac{1}{\sqrt{m_{0\mathrm{k}} + m_{\rho\mathrm{k}}\,\rho + m_{\eta\rho\mathrm{k}}\,\sqrt{\frac{\eta\rho}{\omega_0}}}} \tag{19}$$

and

$$Q = \frac{1}{\omega_0}\cdot\frac{1}{c_{0\mathrm{k}} + c_{\eta\mathrm{k}}\,\eta + c_{\eta\rho\mathrm{k}}\,\sqrt{\omega_0\,\eta\rho}}, \tag{20}$$

where $m_{x\mathrm{k}}$ and $c_{x\mathrm{k}}$ are coefficients and $m_{\rho\mathrm{k}}$ as well as $c_{\eta\mathrm{k}}$ are zero in case of pure one-dimensional shear waves.

4.2.3. Simplified generalized equations

Equation 19 is an implicit equation for ω_0, which makes an exact evaluation of ω_0 for given η and ρ difficult. Therefore, the equations are simplified by considering that the frequency dependence of certain parameters occurring in the analysis is negligible as they are virtually constant within the bandwidth of the resonant system. Doing so, we obtain the following expressions for the angular resonance frequency

$$\omega_0 = \frac{1}{\sqrt{m_{0\mathrm{k}} + m_{\rho\mathrm{k}}\,\rho + m^*_{\eta\rho\mathrm{k}}\,\sqrt{\eta\rho}}} \tag{21}$$

and the quality factor

$$Q = \frac{\sqrt{m_{0\mathrm{k}} + m_{\rho\mathrm{k}}\,\rho + m^*_{\eta\rho\mathrm{k}}\,\sqrt{\eta\rho}}}{c_{0\mathrm{k}} + c_{\eta\mathrm{k}}\,\eta + c^*_{\eta\rho\mathrm{k}}\,\sqrt{\eta\rho}}. \tag{22}$$

Thus if ω_0 and Q for given η and ρ using Eqs. 19 and 20 have to be calculated, numerical, (e.g., iterative) methods can be used. Alternatively, the above simplified expressions give remedy. Conversely, if η and ρ have to be determined from measured $f_\mathrm{r} = \omega_0/(2\,\pi)$ and Q, Eqs. 19 and 20 can be used directly.

The advantage of such reduced order models is that in comparison with completely closed form models, only a few variables have to be determined by means of a parameter fit.

In Sec. 5 these models are fit to experimental results. By means of a comparison of the fitted models it will be shown that the generalized models fit the measured data better than the model considering shear waves only. This supposedly is due to the fact that in addition to one dimensional shear waves, spurious effects such as liquid trapping [22, 23] may be present.

4.3. Electrical model

4.3.1. Excitation torque

The Lorentz force on a charge q moving with velocity $\mathbf{v}$ in the presence of a magnetic field with magnetic flux density $\mathbf{B}$ and an electric field $\mathbf{E}$ is (bold variables denote vectors) [24]

$$\mathbf{F}_\mathrm{L} = q\,(\mathbf{v}\times\mathbf{B} + \mathbf{E}). \tag{23}$$

Assuming perpendicular conditions between the excitation current I_ex, i.e. the charges moving in a wire of length l_r, and the external magnetic field, it follows that the force acting on the wire is given by

$$\underline{F}_\mathrm{ex} = B\,l_\mathrm{r}\,\underline{I}_\mathrm{ex}. \tag{24}$$

With this, the excitation torque can be expressed as

$$\underline{M}_\mathrm{ex} \approx 2\,N\,B\,r_\mathrm{r}\,l_\mathrm{r}\,\underline{I}_\mathrm{ex} \tag{25}$$

where N is the number of turns of the excitation coil and r_r is the radius of the coil, see Fig. 7.

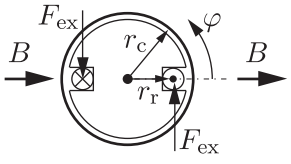

Figure 7: Rotor cross section

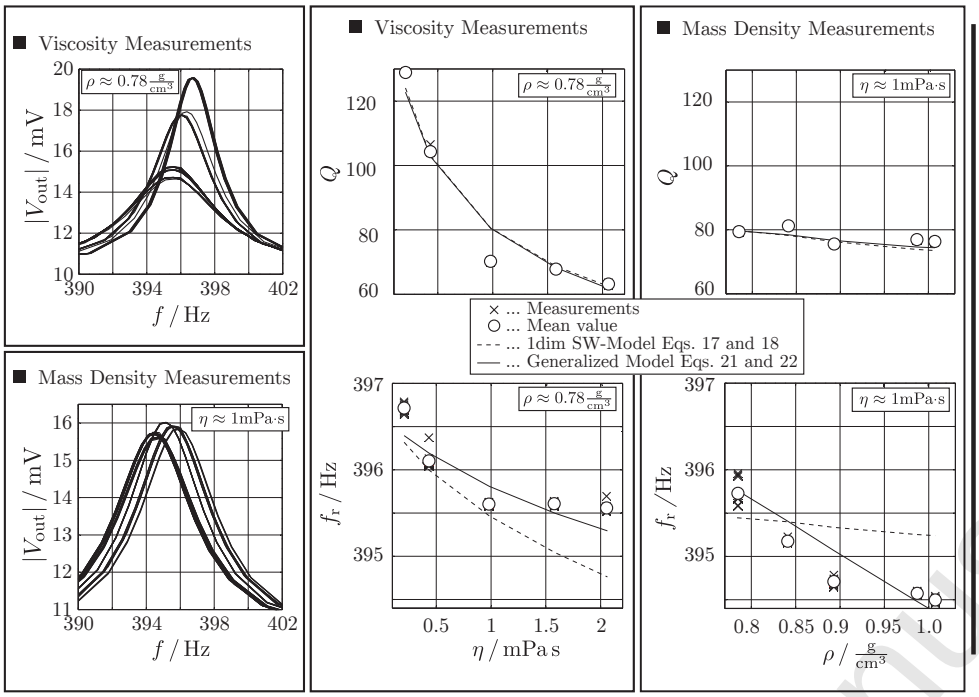

$$f_{\mathrm{r}} = \frac{1}{2\,\pi}\frac{1}{\sqrt{J_{0\mathrm{k}} + J_{\eta\rho\mathrm{k}}\sqrt{\eta\,\rho}}}$$

$$Q = \frac{\sqrt{J_{0\mathrm{k}} + J_{\eta\rho\mathrm{k}}\sqrt{\eta\,\rho}}}{c_{0\mathrm{k}} + c_{\eta\rho\mathrm{k}}\sqrt{\eta\,\rho}}$$

$J_{0\mathrm{k}}/\mathrm{s}^2$	$J_{\eta\rho\mathrm{k}}/\frac{\mathrm{m}^2}{\mathrm{kg}}\cdot\mathrm{s}^{5/2}$
$1.61\cdot10^{-7}$	$1.48\cdot10^{-9}$
$c_{0\mathrm{k}}/\mathrm{s}$	$c_{\eta\rho\mathrm{k}}/\frac{\mathrm{m}^2}{\mathrm{kg}}\cdot\mathrm{s}^{3/2}$
$1.73\cdot10^{-6}$	$3.73\cdot10^{-6}$

$$f_{\mathrm{r}} = \frac{1}{2\,\pi}\frac{1}{\sqrt{m_{0\mathrm{k}} + m_{\rho\mathrm{k}}\,\rho + m^*_{\eta\rho\mathrm{k}}\sqrt{\eta\,\rho}}}$$

$$Q = \frac{\sqrt{m_{0\mathrm{k}} + m_{\rho\mathrm{k}}\,\rho + m^*_{\eta\rho\mathrm{k}}\sqrt{\eta\,\rho}}}{c_{0\mathrm{k}} + c_{\eta\mathrm{k}}\,\eta + c^*_{\eta\rho\mathrm{k}}\sqrt{\eta\,\rho}}$$

$m_{0\mathrm{k}}/\mathrm{s}^2$	$m_{\rho\mathrm{k}}/\frac{\mathrm{m}^3\cdot\mathrm{s}^2}{\mathrm{kg}}$	$m^*_{\eta\rho\mathrm{k}}/\frac{\mathrm{m}^2}{\mathrm{kg}}\cdot\mathrm{s}^{5/2}$
$1.57\cdot10^{-7}$	$4.65\cdot10^{-12}$	$1.06\cdot10^{-9}$
$c_{0\mathrm{k}}/\mathrm{s}$	$c_{\eta\mathrm{k}}/\frac{\mathrm{m}\cdot\mathrm{s}^2}{\mathrm{kg}}$	$c^*_{\eta\rho\mathrm{k}}/\frac{\mathrm{m}^2}{\mathrm{kg}}\cdot\mathrm{s}^{3/2}$
$1.89\cdot10^{-6}$	$2.12\cdot10^{-4}$	$3.31\cdot10^{-6}$

Figure 8: Measured amplitudes as well as evaluated resonance frequencies and quality factors for two liquid series. The one dimensional shear wave model as well as the generalized model are fit to the measured data. The model parameters are given on the right hand side.

4.3.2. Motion induced voltage

Using Faraday's law of induction and the equation for Lorentz forces, the motion induced voltage on the coil can be expressed as:

$$V_{\mathrm{M}}(t) = -\int_{\mathrm{coil}} (\mathbf{v}\times\mathbf{B})\cdot\mathrm{d}\mathbf{s}. \tag{26}$$

Assuming the magnetic flux density to be symmetric in the air gap, constant along the coil's length and aligned in parallel with the coil for $\varphi = 0$, see Fig. 7, it follows

$$V_{\mathrm{M}}(t) = 2\,N\,r_{\mathrm{r}}\cos\varphi\,\frac{\mathrm{d}\varphi}{\mathrm{d}t}\,B\,l_{\mathrm{r}}. \tag{27}$$

For small twisting angles, the motion induced voltage in the frequency domain using the angular speed Eq. 16 reads

$$\underline{V}_{\mathrm{M}}(\omega) \approx 2\,N\,r_{\mathrm{r}}\,B\,l_{\mathrm{r}}\,\underline{\Omega}(\omega). \tag{28}$$

This equation for the motion induced voltage is used for modeling the measurable output voltage V_{out} for the single as well as for the double coil setup in Eqs. 1 and 2.

5. Experimental investigation

5.1. Measurements in liquids

The demonstrator discussed in Sec. 3 has been used to experimentally test the principle operation of such a torsional resonator in liquids and to investigate the effect of different mass densities and viscosities on recorded frequency responses. Amplitudes as well as evaluated quality factors and resonance frequencies for two different sets of liquid series are depicted in Fig. 8. There, the results of the fitted models performing a linear fitting procedure, see [25], for $f_{\mathrm{r}} = \omega_0/(2\,\pi)$ and Q using Eqs. 17, 18, 21 and, 22 are depicted as well. The values for the examined liquids' viscosities η and mass densities ρ (which were determined with an Anton Paar SVM 3000) as well as the mean values of the associated, evaluated resonance frequencies f_{r} and quality factors Q are given in Tab. 1. The SVM 3000 features a reproducibility of 0.35 % for viscosity and 0.0005 g/cm^3 for mass density. The measurements were performed at 25 °C. The values for f_{r} and Q were evaluated from the recorded frequency responses using a fitting algorithm described in [26]. The used liquid series are the so-called viscosity series and mass density series in the following. The first is a mixture of isopropanol and acetone covering a viscosity range of 0.21 mPa·s to 2.05 mPa·s for mass densities of roughly 0.78 g/cm^3. The percentage of mass isopropanol m_{I} and mass acetone m_{A} is given in the left column of Tab. 1. The mass density series cover a range of mass densities of 0.79 g/cm^3 to 1.01 g/cm^3 for viscosities of roughly 1 mPa·s and were prepared using acetone, isopropanol, ethanol, DI-water and glycerol. After mixing, the liquids were investigated with the SVM 3000. These two liquid series are used to separately investigate experimentally the effect of varying viscosities or mass densities on f_{r} and Q.

The results obtained with both liquid series clearly show the effect of mass density and viscosity on the experimentally obtained values for f_{r} and Q. Deviations of the measured from the modeled values as well as slight variations in f_{r} and Q can be observed. These supposedly originate from imperfections in the prototype setup. These imperfections are associated with the fact that first, during cleaning and refilling of the sensor, the

Viscosity Series $T = 25°C$										
$\frac{m_I}{m_A+m_I}$ / %	η/(mPa·s)	ρ/(g/cm^3)	f_r/Hz	Q	$\hat{\eta}$/(mPa·s)	$\Delta\eta$/(mPa·s)	$\Delta\eta_{rel}$	$\hat{\rho}$/(g/cm^3)	$\Delta\rho$/(g/cm^3)	$\Delta\rho_{rel}$
0	0.207	0.7841	$396.710 \pm 1.4 \cdot 10^{-3}$	129.0 ± 0.44	0.173	-0.034	-0.164	0.7394	-0.0447	-0.057
51	0.433	0.7790	$396.103 \pm 3.3 \cdot 10^{-3}$	104.4 ± 0.04	0.399	-0.034	-0.079	0.7985	0.0195	0.025
83	0.980	0.7793	$395.599 \pm 0.3 \cdot 10^{-3}$	70.3 ± 0.16	1.464	0.484	0.493	0.7730	-0.0063	-0.008
95	1.576	0.7803	$395.605 \pm 3.5 \cdot 10^{-3}$	67.8 ± 0.03	1.636	0.059	0.038	0.7602	-0.0201	-0.026
100	2.054	0.7804	$395.56 \pm 4.8 \cdot 10^{-3}$	63.3 ± 0.36	2.006	-0.049	-0.024	0.7444	-0.0360	-0.046

Density Series $T = 25°C$									
η/(mPa·s)	ρ/(g/cm^3)	f_r/Hz	Q	$\hat{\eta}$/(mPa·s)	$\Delta\eta$/(mPa·s)	$\Delta\eta_{rel}$	$\hat{\rho}$/(g/cm^3)	$\Delta\rho$/(g/cm^3)	$\Delta\rho_{rel}$
1.006	0.7849	$395.729 \pm 0.8 \cdot 10^{-3}$	79.4 ± 0.15	1.009	0.003	0.003	0.7894	0.0045	0.006
0.994	0.8411	$395.177 \pm 1.4 \cdot 10^{-3}$	81.2 ± 0.31	0.850	-0.144	-0.145	0.8918	0.0507	0.060
1.010	0.8931	$394.706 \pm 10.5 \cdot 10^{-3}$	76 ± 2.2	0.999	-0.011	-0.011	0.9513	0.0582	0.065
1.006	0.9870	$394.574 \pm 8.6 \cdot 10^{-3}$	77 ± 2.4	0.925	-0.080	-0.080	0.9798	-0.0072	-0.007
0.998	1.0073	$394.500 \pm 5.5 \cdot 10^{-3}$	76 ± 1.3	0.937	-0.061	-0.061	0.9904	-0.0169	-0.017

Table 1: Upper part: Acetone-isopropanol solutions for viscosity measurements. Lower part: Solutions for mass density measurements. The plus-minus values are evaluated typical errors (single standard deviations). $\hat{x}$ are the calculated values for viscosity and mass density using Eqs. 19 and 20 and evaluated mean values for f_r and Q. $\Delta x = \hat{x} - x$ and $\Delta x_{rel} = \Delta x/x$ are absolute and relative deviations from the values for viscosity and mass density, respectively.

resonator may have been detuned due to an insufficiently stable clamping, second, the open experimental well, which allows evaporation of the liquid during the measurements, and third, geometrical imperfections such as e.g., surface roughnesses and a not perfect alignment of the oscillating cylinder with the torsional springs. For Q, both models yield approximately the same results, where for f_r, the generalized model clearly yields better results. This finding can be explained by surface roughness, which yields so-called liquid trapping [22, 23] and thus a higher sensitivity to mass density. This effect might be beneficial, as the effect of η and ρ on f_r and Q cannot be separated with devices yielding pure one-dimensional shear waves without liquid trapping.

Despite the discussed drawbacks in the presented setup, a rough estimation of the device's sensitivity can be made. We define the relative sensitivity of a quantity $X(y_i)$ to an independent variable y_i as

$$S_{X,y_i} = \left| \frac{\partial X}{\partial y_i} \cdot \frac{y_i}{X} \right| \tag{29}$$

where X either stands for f_r or Q and y_i for η and ρ, yielding four different sensitivities which are evaluated from the fitted generalized model Eqs. 21 and 22. The four sensitivities $S_{f_r,\eta}$, $S_{f_r,\rho}$, $S_{Q,\eta}$ and $S_{Q,\rho}$ are not constant but depend on η as well as on ρ and thus are depicted as bands in Fig. 9 for the experimentally evaluated range of viscosities and mass densities. The upper boundary of the bands in the plots on the left hand side (i.e., $S_{f_r,\eta}$ and $S_{Q,\eta}$) are the values for $\rho = 1.01\,\mathrm{g/cm^3}$, the lower boundary for $\rho = 0.79\,\mathrm{g/cm^3}$. On the right hand side (i.e., $S_{f_r,\rho}$ and $S_{Q,\rho}$) the upper and lower boundaries of the bands represent the evaluated values for $\eta = 0.21\,\mathrm{mPa{\cdot}s}$ and $\eta = 2.05\,\mathrm{mPa{\cdot}s}$, respectively. In Fig. 9 the sensitivities obtained with the torsional resonator are depicted in comparison with the sensitivities achieved with circular and rectangular cross sectioned steel tuning forks oscillating at 400 Hz in liquids approximately, a U-shaped wire sensor ($f_r \approx 930\,\mathrm{Hz}$) [27], and a quartz tuning fork ($f_r \approx 32.7\,\mathrm{kHz}$) [13].

5.2. Measurement accuracy

Equations 19 and 20 were used to calculate η and ρ for evaluated f_r and Q. The fitted model parameters using a linear fitting procedure described in [21, 25] are given in Tab. 2. Despite their limited accuracy, the mean values for f_r and Q given in Tab. 1 are used to calculate the values for viscosity and mass density for both liquid series. The evaluation of absolute and relative errors given in Tab. 1 shows that with the present setup, absolute and relative accuracies for viscosity in the range of $[|\Delta\eta|_{min}, |\Delta\eta|_{max}] = [0.003, 0.484]$ mPa·s and $[|\Delta\eta_{rel}|_{min}, |\Delta\eta_{rel}|_{max}] = [0.003, 0.493]$, respectively are obtained. For the calculated mass densities the obtained accuracies are $[|\Delta\rho|_{min}, |\Delta\rho|_{max}] = [0.0045, 0.0058]$ g/cm^3 and $[|\Delta\rho_{rel}|_{min}, |\Delta\rho_{rel}|_{max}] = [0.005, 0.065]$. This evaluation substantiates the need for setup improvement, especially to obtain

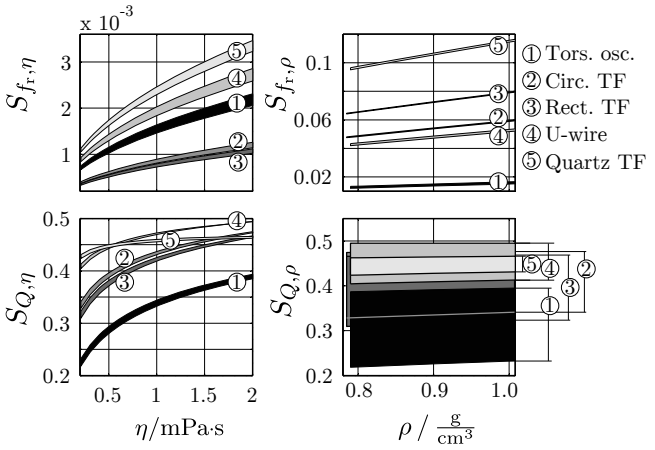

Figure 9: Sensitivities to viscosity and mass density: The sensitivities of f_r and Q to η and ρ are not constant but dependent both on η and ρ. For this reason the sensitivities are depicted as bands, in the experimentally investigated range of viscosities and mass densities. In the plots for $S_{f_r,\eta}$ and $S_{Q,\eta}$ the upper boundary of the bands are the values for $\rho = 1.01\,\mathrm{g/cm^3}$, the lower boundary for $\rho = 0.79\,\mathrm{g/cm^3}$. In the plots for $S_{f_r,\rho}$ and $S_{Q,\rho}$ the upper and lower boundaries of the bands represent the evaluated values for $\eta = 0.21\,\mathrm{mPa{\cdot}s}$ and $\eta = 2.05\,\mathrm{mPa{\cdot}s}$, respectively.

m_{0k}/s^2	$m_{\rho k}/\frac{\mathrm{m}^3\cdot\mathrm{s}^2}{\mathrm{kg}}$	$m_{\eta\rho k}/\frac{\mathrm{m}^2}{\mathrm{kg}}\cdot\mathrm{s}^2$
$1.57\cdot10^{-7}$	$4.64\cdot10^{-12}$	$5.29\cdot10^{-8}$
c_{0k}/s	$c_{\eta k}/\frac{\mathrm{m}\cdot\mathrm{s}^2}{\mathrm{kg}}$	$c_{\eta\rho k}/\frac{\mathrm{m}^2}{\mathrm{kg}}\cdot\mathrm{s}^2$
$1.88\cdot10^{-6}$	$1.93\cdot10^{-4}$	$6.73\cdot10^{-8}$

Table 2: Fitted model parameters using Eqs. 19 and 20.

more accurate measurement results for viscosity. However, the purpose of this work was a feasibility study of torsional, resonant viscosity and mass density sensors, their modeling and first designs of promising demonstrators. In [28] the advantages and capability of resonant viscosity and mass density sensors using conventional steel tuning forks with circular and rectangular cross sections was demonstrated.

5.3. Cross sensitivity to temperature

Mechanical resonators can show a significant dependence of their resonance frequency to temperature. This dependence is mainly due to the thermal expansion of the resonator and the temperature dependence of the resonator's Young's modulus. For doubly clamped structures such e.g. bridges [15, 29] and straight wire resonators [30, 31], the cross sensitivity of the resonance frequency to temperature becomes large if significant thermal pre-stresses are induced. The dependence of the resonance frequency to temperature can be positive as well as negative. In [32], micro-machined vibrating strings are used as ultrasensitive temperature sensors. For the case of resonant viscosity sensors, this cross sensitivity directly limits the sensor's accuracy and thus should be kept as low as possible. The dependence of the torsional resonator's resonance frequency has been evaluated in a temperature range from 5 °C to 60 °C in 5 °C temperature steps. Figure 10 shows the magnitude of measured frequency responses as well as evaluated resonance frequencies at these temperatures. In Tab. 3 a comparison of the resonance frequency's dependence to temperature is given for different resonators. The first five sensors, i.e a U-shaped tungsten wire sensor, U (W), [27], a U-shaped gold coated silicon resonator, U(Si, Au), [33], a steel tuning fork, TF (steel), a silicon cantilever, CL (Si), [34] and a gold coated silicon cantilever, CL (Si, Au), [35] are singly clamped structures and thus show a relatively small dependence of the resonance frequency to temperature. The last two sensors i.e., the torsional resonator, TR, and a straight tungsten wire sensor, SW (W), [31] are doubly clamped structures and thus, show a much higher dependence of the resonance frequency to temperature. However, this dependence is much lower for the torsional resonator compared to the straight wire sensor. To reduce this cross sensitivity, using only one torsional spring instead of two may be a possible approach.

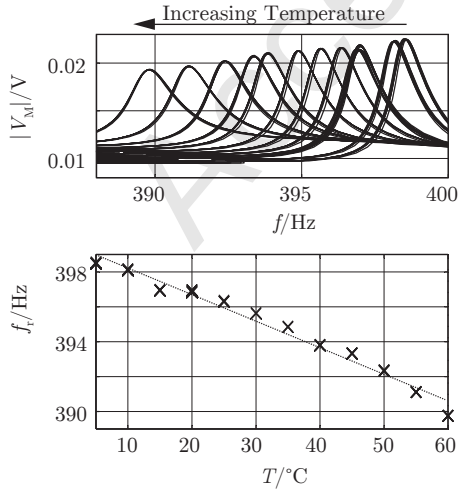

Figure 10: Cross sensitivity of the resonance frequency to temperature. The upper figure shows the magnitudes of recorded frequency responses, the lower figure evaluated resonance frequencies versus temperature.

Sensor	f_0 kHz	$\Delta f_r/\Delta T$ (Hz/K)	$\Delta f_{r,rel}/\Delta T$ (1/K)	Ref.
U (W)	0.95	-0.048	$-60\cdot10^{-6}$	[27]
U (Si, Au)	5.96	-0.441	$-69\cdot10^{-6}$	[33]
TF (Steel)	0.44	-0.0519	$-118\cdot10^{-6}$	t.w.
CL (Si)	43.83	-1.3	$-29.7\cdot10^{-6}$	[34]
CL (Si, Au)	18.33	-1.83	$-100\cdot10^{-6}$	[35]
TR	0.4	-0.15	$-385.58\cdot10^{-6}$	t.w.
SW (W)	2.98	30	0.01	[31]

Table 3: Cross sensitivities of the resonance frequency (fundamental mode) to temperature. f_0: nominal resonance frequency, $\Delta f_r = f_r(T_0) - f_r(T_1)$: resonance frequency shift, $\Delta T = T_0 - T_1$ difference of temperatures T_0 and T_1, $\Delta f_{r,rel} = \Delta f_r/f_0$: relative resonance frequency shift, 't.w.' designates this work.

6. Conclusion and outlook

A first study of the electromagnetically driven and read out torsional oscillator in air showed the advantages of using one single coil for both, excitation and readout. The advantages are mainly based on the manufactural benefit that in case of using one coil (instead of two) only two wires have to be electrically connected for power supply and readout which in this case is implemented by contacting the torsional springs. The feasibility of such a torsional resonator for viscosity and mass density sensing applications has been shown by measurements in ten different liquids. For design purposes, a complete analytical model comprising the structural and fluid mechanics and relating output to input signals has been elaborated. Therefrom, reduced order models have been derived which relate resonance frequency and quality factor to viscosity and mass density, respectively. The advantage of such models is that only four to six factors have to be determined to describe the sensors characteristics. The comparison of both fitted model results shows that the generalized model yields significantly better results for f_r which can be explained by liquid trapping due to surface roughnesses of the cylinder shell. A first estimation of the device's sensitivity and its cross sensitivity of its resonance frequency has been made and compared to other resonant viscosity and mass density sensors.

Regarding future work, a more reliable clamping and housing has to be designed and manufactured aiming to obtain more stable and accurate results. By means of further experiments, the maximum measurable viscosities and resolution have to be investigated.

Acknowledgment

This work has been partially supported by the Linz Center of Mechatronics (LCM) in the framework of the Austrian COMET-K2 program. We also want to thank Bernhard Mayrhofer and Johann Katzenmayer for their help and excellent assistance.

References

[1] B. Jakoby, R. Beigelbeck, F. Keplinger, F. Lucklum, A. Niedermayer, E. K. Reichel, C. Riesch, T. Voglhuber-Brunnmaier, B. Weiss, Miniaturized sensors for the viscosity and density of liquids – performance and issues, IEEE transactions on ultrasonics, ferroelectrics, and frequency control 57 (1) (2010) 111–120. doi:10.1109/TUFFC.2010.1386.

[2] E. K. Reichel, C. Riesch, F. Keplinger, C. E. A. Kirschhock, B. Jakoby, Analysis and experimental verification of a metallic suspended plate resonator for viscosity sensing, Sensors and Actuators A: Physical 162 (2010) 418–424. doi:10.1016/j.sna.2010.02.017.

[3] A. Abdallah, M. Heinisch, B. Jakoby, Measurement error estimation and quality factor improvement of an electrodynamic-acoustic resonator sensor for viscosity measurement, Sensors and Actuators A: Physical 199 (2013) 318–324.

[4] C. Riesch, E. K. Reichel, A. Jachimowicz, J. Schalko, P. Hudek, B. Jakoby, F. Keplinger, A suspended plate viscosity sensor featuring in-plane vibration and piezoresistive readout, J. Micromech. Microeng. 19 (2009) 075010. doi:10.1088/0960-1317/19/7/075010.

[5] S. Cerimovic, R. Beigelbeck, H. Antlinger, J. Schalko, B. Jakoby, F. Keplinger, Sensing viscosity and density of glycerol–water mixtures utilizing a suspended plate mems resonator, Microsystem technologies 18 (7-8) (2012) 1045–1056.

[6] S. J. Martin, V. E. Granstaff, G. C. Frye, Characterization of a quartz crystal microbalance with simultaneous mass and liquid loading, Anal. Chem. 63 (1991) 2272–2281.

[7] R. Beigelbeck, B. Jakoby, A two-dimensional analysis of spurious compressional wave excitation by thickness-shear-mode resonators, Journal of applied physics 95 (9) (2004) 4989–4995.

[8] T. Voglhuber-Brunnmaier, B. Jakoby, Efficient spectral domain formulation of loading effects in acoustic sensors, Sensors and Actuators A: Physical 186 (2012) 38–47.

[9] C. W. Macosko, Rheology, Principles, Measurements and Applications, Wiley- VCH, 1994.

[10] A. Rahafrooz, S. Pourkamali, Characterization of rotational mode disk resonator quality factors in liquid, Frequency Control and the European Frequency and Time Forum (FCS), 2011 Joint Conference of the IEEE International (2011) 5 pages.

[11] I. Dufour, A. Maali, Y. Amarouchene, et al., The microcantilever: A versatile tool for measuring the rheological properties of complex fluids, Journal of Sensors 2012. doi:10.1155/2012/719898.

[12] C. Vančura, I. Dufour, S. M. Heinrich, F. Josse, A. Hierlemann, Analysis of resonating microcantilevers operating in a viscous liquid environment, Sensors and Actuators A: Physical 141 (1) (2008) 43–51.

[13] J. Toledo, T. Manzaneque, J. Hernando-García, J. Vázquez, A. Ababneh, H. Seidel, M. Lapuerta, J. Sánchez-Rojas, Application of quartz tuning forks and extensional microresonators for viscosity and density measurements in oil/fuel mixtures, Microsystem Technologies (2014) 1–9.

[14] C. Riesch, A. Jachimowicz, F. Keplinger, E. K. Reichel, B. Jakoby, A novel sensor system for liquid properties based on a micromachined beam and a low-cost optical readout, Proceedings IEEE Sensors (2007) 872–875.

[15] I. Etchart, H. Chen, P. Dryden, J. Jundt, C. Harrison, K. Hsu, F. Marty, B. Mercier, Mems sensors for density–viscosity sensing in a low-flow microfluidic environment, Sensors and Actuators A: Physical 141 (2) (2008) 266–275.

[16] M. Heinisch, T. Voglhuber-Brunnmaier, E. K. Reichel, S. Clara, A. Abdallah, B. Jakoby, Concept study on an electrodynamically driven and read-out torsional oscillator, Proceedings Microelectronic Systems Symposium (2014).

[17] W. W. Weaver, S. P. Timoshenko, D. H. Young, Vibration Problems in Engineering, 5th Edition, Wiley, 1990.

[18] L. D. Landau, E. M. Lifshitz, Fluid Mechanics, Butterworth-Heinemann, 1987.

[19] M. Heinisch, E. K. Reichel, B. Jakoby, A suspended plate in-plane resonator for rheological measurements at tunable frequencies, in: Proc. Sensor + Test, 2011, pp. 61– 66.

[20] M. Baù, V. Ferrari, D. Marioli, A. Taroni, Cost-effective system for the characterization of microstructures vibrating in out-of-plane modes, Sensors and Actuators A: Physical 142 (1) (2008) 270–275.

[21] M. Heinisch, T. Voglhuber-Brunnmaier, E. K. Reichel, I. Dufour, B. Jakoby, Reduced order models for resonant viscosity and mass density sensors, Sens. Actuators A: Physical 220 (2014) 76–84.

[22] S. J. Martin, R. W. Cernosek, J. J. Spates, Sensing liquid properties with shear-mode resonator sensors, Transducers, Eurosensors IX (1995) 712–715.

[23] B. Jakoby, M. Vellekoop, Physical sensors for liquid properties, IEEE sensors journal 11 (12) (2011) 3076–3085.

[24] D. J. Griffiths, Introduction to Electrodynamics, Pearson, 2013.

[25] E. K. Chong, S. H. Zak, An introduction to optimization, 2nd Edition, John Wiley & Sons, 2001.

[26] A. O. Niedermayer, T. Voglhuber-Brunnmaier, J. Sell, B. Jakoby, Methods for the robust measurement of the resonant frequency and quality factor of significantly damped resonating devices, Measurement Science and Technology 23 (8) (2012) 085107.

[27] M. Heinisch, E. K. Reichel, I. Dufour, B. Jakoby, A u-shaped wire for viscosity and mass density sensing, Sens. Actuators A: Phys. 214 (2014) 245–251.

[28] M. Heinisch, T. Voglhuber-Brunnmaier, E. K. Reichel, I. Dufour, B. Jakoby, Application of resonant steel tuning forks with circular and rectangular cross sections for precise mass density and viscosity measurements, Manuscript submitted at Sensors and Actuators A: Physical (2015).

[29] C. Riesch, Micromachined Viscosity Sensors, Shaker Verlag, 2009.

[30] D. Seibt, Schwingdrahtviskosimeter mit integriertem ein-senkkörperdichtemessverfahren für untersuchungen an gasen in größeren temperatur- und druckbereichen, Ph.D. thesis, Universität Rostock (2007).

[31] M. Heinisch, E. K. Reichel, I. Dufour, B. Jakoby, Tunable resonators in the low khz range for viscosity sensing, Sensors and Actuators A: Physical 186 (2012) 111–117. doi:http://dx.doi.org/10.1016/j.sna.2012.03.009.

[32] T. Larsen, S. Schmid, L. Grönberg, A. O. Niskanen, J. Hassel, S. Dohn, A. Boisen, Ultrasensitive string-based temperature sensors, Applied Physics Letters 98 (12) (2011) 121901.

[33] M. Stifter, T. Sauter, W. Hortschitz, F. Keplinger, H. Steiner, Mems heterodyne amf detection with capacitive sensing, Proceedings IEEE Sensors 2012 (2012) 1–4doi:10.1109/ICSENS.2012.6411171.

[34] H. S. Wasisto, S. Merzsch, A. Waag, E. Uhde, T. Salthammer, E. Peiner, Airborne engineered nanoparticle mass sensor based on a silicon resonant cantilever, Sensors and Actuators B: Chemical 180 (2013) 77–89.

[35] R. Sandberg, W. Svendsen, K. Mølhave, A. Boisen, Temperature and pressure dependence of resonance in multi-layer microcantilevers, Journal of Micromechanics and Microengineering 15 (8) (2005) 1454.

Biographies

Martin Heinisch obtained his Dipl.-Ing. (M.Sc.) in Mechatronics from Johannes Kepler University Linz, Austria, in 2009. After his Master studies he went to the University of California, Los Angeles (U.C.L.A.) as a Marshall Plan Scholarship grantee, where he did research in the field of microfluidic applications and self assembling systems. In 2010 he started a Ph.D. program at the Institute for Microelectronics and Microsensors of the Johannes Kepler University Linz, Austria where he is currently working on resonating liquid sensors.

Thomas Voglhuber-Brunnmaier received the Dipl.-Ing. (M.Sc.) degree in Mechatronics in 2007 and the Dr.techn. (Ph.D.) in May 2013 at the Institute for Microelectronics and Microsensors (IME) at the Johannes Kepler University (JKU) in Linz,

Austria. From May 2013 he holds a PostDoc position at the Center for Integrated Sensor Systems (CISS) at the Danube University Krems (DUK), where he works in close cooperation with IME on fluid sensors. His fields of interest are the modeling of micro-sensors, statistical signal processing, numerical methods and analog electronics.

Erwin K. Reichel was born in Linz, Austria, in 1979. He received the Dipl.-Ing. (M.Sc.) degree in mechatronics from Johannes Kepler University, Linz, Austria, in 2006. From 2006 to 2009 he was working on the Ph.D. thesis at the Institute for Microelectronics and Microsensors of the Johannes Kepler University, Linz and graduated in October 2009. Afterwards he held a post-doctoral position at the Centre for Surface Chemistry and Catalysis as well as at the Department for Chemical Engineering, KU Leuven, Belgium until June 2012. Since then he holds a position as university assistant at the Johannes Kepler University Linz. The main research fields are the modeling, design, and implementation of sensors for liquid properties, and monitoring of phase transition in complex solutions.

Isabelle Dufour graduated from Ecole Normale Supérieure de Cachan in 1990 and received the Ph.D. and H.D.R. degrees in engineering science from the University of Paris-Sud, Orsay, France, in 1993 and 2000, respectively. She was a CNRS research fellow from 1994 to 2007, first in Cachan working on the modelling of electrostatic actuators (micromotors, micropumps) and then after 2000 in Bordeaux working on microcantilever-based chemical sensors. She is currently Professor of electrical engineering at the University of Bordeaux and her research interests are in the areas of microcantilever-based sensors for chemical detection, rheological measurements and materials characterisation.

Bernhard Jakoby obtained his Dipl.-Ing. (M.Sc.) in Communication Engineering and his doctoral (Ph.D.) degree in electrical engineering from the Vienna University of Technology (VUT), Austria, in 1991 and 1994, respectively. In 2001 he obtained a venia legendi for Theoretical Electrical Engineering from the VUT. From 1991 to 1994 he worked as a Research Assistant at the Institute of General Electrical Engineering and Electronics of the VUT. Subsequently he stayed as an Erwin Schrödinger Fellow at the University of Ghent, Belgium, performing research on the electrodynamics of complex media. From 1996 to 1999 he held the position of a Research Associate and later Assistant Professor at the Delft University of Technology, The Netherlands, working in the field of microacoustic sensors. From 1999 to 2001 he was with the Automotive Electronics Division of the Robert Bosch GmbH, Germany, where he conducted development projects in the field of automotive liquid sensors. In 2001 he joined the newly formed Industrial Sensor Systems group of the VUT as an Associate Professor. In 2005 he was appointed Full Professor of Microelectronics at the Johannes Kepler University Linz, Austria. He is currently working in the field of liquid sensors and monitoring systems.

List of Figures